Lineshapes of dynamical correlation functions in Heisenberg chains

Ralph Werner
Physics Department, Brookhaven National Laboratory, Upton, New York 11973-5000

Andreas Klümper
Physics Department, University of Dortmund, D-44221 Dortmund, Germany

(Received 6 April 2001; revised manuscript received 11 July 2001; published 10 October 2001)

We calculate lineshapes of correlation functions by use of complete diagonalization data of finite chains and analytical implications from conformal-field theory, density of states, and Bethe ansatz. The numerical data have different finite-size accuracy in the cases of the imaginary and real parts in the frequency and time representations of spin-correlation functions, respectively. The low-temperature, conformally invariant regime crosses over at $T^* \approx 0.7J$ to a diffusive regime that in turn connects continuously to the high-temperature, interacting-fermion regime. The first-moment sum rule is determined.

DOI: 10.1103/PhysRevB.64.174414 PACS number(s): 75.10.Jm, 75.40.Gb

I. INTRODUCTION

Dynamical correlations characterize the spectral properties of physical systems. They are accessible by a multitude of experimental setups. The access to dynamical correlation functions for physically relevant systems is usually difficult even in exactly solvable models.[1,2] Dynamical spin-correlation functions in Heisenberg chains have been widely studied. Numerically, the dynamics at $T=0$ are accessible by Lanczos and continued fraction techniques, which have been applied to Heisenberg chains with dimerization[3] and additional frustration.[4,5] Dynamics of frustrated quantum-spin systems in magnetic fields were studied[6] as well as a spin system coupled to a dynamical phonon.[7] At finite temperatures partially anisotropic Heisenberg chains[8] and chains with frustration[9] were studied by complete diagonalization of finite systems. The Heisenberg chain was also studied by a combination of high-temperature expansions with quantum Monte Carlo simulations.[10] The analytical investigation of dynamical spin-correlation functions usually involves the Bethe ansatz or implications from conformal-field theory.[11–13] The comparison of numerical and approximate analytical results for the purpose of accuracy control has been used in various previous approaches.[14–20]

Usually the focus lies on the imaginary part of the correlation functions. The real and the imaginary parts can be Kramers-Kronig transformed into each other and thus hold the same information. This is also true for the Fourier transform. The information that can be extracted from finite systems accessible by exact diagonalization concerning the thermodynamic limit is limited. The accuracy of the results is different for different representations. In the case of finite systems it proves thus useful to actually calculate all three representations to extrapolate to the thermodynamic limit.[21]

The dynamical correlation functions become system size independent for high excitation energies[21] or, equivalently, on short time scales.[8] While finite systems thus allow for the determination of correlation functions in the thermodynamic limit at high frequencies or on short time scales, field-theoretical results describe their asymptotic behavior on long time scales or for small frequencies.[12,13] The perspective of this paper is to combine the strongholds of both methods.

The system to be discussed here is the one-dimensional antiferromagnetic Heisenberg model

$$H=\sum_l \left(JS_l^xS_{l+1}^x+JS_l^yS_{l+1}^y+J_zS_l^zS_{l+1}^z\right) + J_2\sum_l \left(S_l^xS_{l+2}^x+S_l^yS_{l+2}^y+S_l^zS_{l+2}^z\right) \tag{1}$$

with the superexchange integrals J and J_2 between nearest-neighbor and next-nearest-neighbor magnetic ions, respectively, z-axis anisotropy J_z and spin-1/2 operator components S_l^ν with $\nu=x,y,z$ at site l. Energies will be given in units of the in-plane exchange, i.e., $J\equiv 1$. This Hamiltonian is relevant for the description of the magnetic systems in many quasi-one-dimensional materials as Sr_2CuO_3,[22,23] Cs_2CuCl_4,[24] $KCuF_3$,[25] or $CuGeO_3$.[26]

We focus on the spin-correlation function

$$\chi(q,i\omega_n)=\frac{1}{L}\int_0^\beta d\tau\, e^{i\omega_n\tau}\langle S_q^z(\tau)S_{-q}^z(0)\rangle \tag{2}$$

with Matsubara frequencies $\omega_n=2\pi n/\beta$, inverse temperature $\beta=1/T$, $(k_B\equiv 1)$, Fourier transformed spin operators in interaction representation $S_q^z(\tau)=e^{-H\tau}\Sigma_l e^{-iql}S_l^z e^{H\tau}$, and number of sites L. In its analytically continued form, where $i\omega_n\to\omega+i\epsilon$ with $\epsilon\to 0$, it determines the structure factor

$$S(q,\omega)=\frac{1}{\pi}\frac{\mathrm{Im}\,\chi(q,\omega)}{1-e^{-\beta\omega}} \tag{3}$$

relevant for neutron scattering experiments.

A. Numerical methods

For finite systems the correlation function can be calculated through the diagonalization of the spin Hamiltonian in the spectral representation since eigenfunctions $|n\rangle$ and eigenvalues E_n are known. All numerical results in this paper are obtained using periodic boundary conditions. Defining the matrix elements

$$V_{nm}=\langle n|S_q^z|m\rangle \tag{4}$$

and the Boltzmann factor

$$f_{nm}(\beta)=\frac{1}{Z}(e^{-\beta E_n}-e^{-\beta E_m}), \tag{5}$$

where $Z=\mathrm{Tr}\, e^{-\beta H}$ is the partition function, one can write

$$\mathrm{Re}\,\chi(q,\omega)=-\lim_{\epsilon\to 0}\sum_{m,n}\frac{f_{nm}(\beta)|V_{nm}|^2(\omega+E_n-E_m)}{(\omega+E_n-E_m)^2+\epsilon^2}, \tag{6}$$

$$\mathrm{Im}\,\chi(q,\omega)=\pi\sum_{m,n} f_{nm}(\beta)|V_{nm}|^2\delta(\omega+E_n-E_m). \tag{7}$$

The corresponding real-time retarded spin-correlation function is obtained via a Fourier transformation as

$$\chi(q,t)=\frac{1}{2\pi}\int_{-\infty}^{\infty}d\omega\;\; e^{-i\omega t}\chi(q,\omega)$$

$$=-i\,\theta(t)\sum_{m,n} f_{nm}(\beta)|V_{nm}|^2 e^{i(E_n-E_m)t}, \tag{8}$$

where $\theta(t)$ is the Heaviside function.

To determine the correlation functions in frequency space we use the same methods as described in Ref. 21 that we briefly summarize. At low temperatures small systems exhibit a small number of dominant spectral lines at frequencies $\tilde{\omega}_j$ that usually can be attributed to specific excitations.[19,20] The imaginary part of the correlation function is determined most accurately by ''binning'' the data as

$$\mathrm{Im}\,\chi(q_z,\tilde{\omega}_j^{\inf}<\omega<\tilde{\omega}_j^{\sup})$$

$$=\pi\sum_{m,n}\frac{f_{nm}(\beta)|V_{nm}|^2[\,\theta(\omega_{nm}-\tilde{\omega}_j^{\inf})-\theta(\omega_{nm}-\tilde{\omega}_j^{\sup})]}{\tilde{\omega}_j^{\sup}-\tilde{\omega}_j^{\inf}}. \tag{9}$$

For small systems at low temperatures the appropriate choice is such that the interval boundaries lie in the middle between the dominant spectral lines, i.e., $\tilde{\omega}_j^{\sup}=\tilde{\omega}_{j+1}^{\inf}=(\tilde{\omega}_j+\tilde{\omega}_{j+1})/2$. If only the ''dominant'' spectral lines are present and if those lines form a well-defined continuum in the thermodynamic limit, i.e., for $L\to\infty$, Karbach, Müller, and coworkers have shown[17,19,20] that Eq. (7) can be used, appropriately scaled to the thermodynamic limit, by introducing a density of states with respect to appropriate quantum numbers derived from Bethe ansatz. This leads to the following representation of the imaginary part of the correlation function:[21]

$$\mathrm{Im}\,\chi(q_z,\tilde{\omega}_j)=\sum_{m,n}^{\tilde{\omega}_j=E_n-E_m}\frac{2\pi\;\; f_{nm}(\beta)|V_{nm}|^2}{\tilde{\omega}_{j+1}-\tilde{\omega}_{j-1}}. \tag{10}$$

The sum covers only values of n and m such that $\tilde{\omega}_j=E_n-E_m$. In Heisenberg chains this representation is only applicable at $T=0$.

It can be shown that Eq. (6) gives very accurate results for the real part of the correlation function if it is evaluated at the dominant spectral lines $\tilde{\omega}_j$.[21]

$$\mathrm{Re}\,\chi(q_z,\tilde{\omega}_j)=-\sum_{m,n}\frac{f_{nm}(\beta)|V_{nm}|^2}{(\tilde{\omega}_j+E_n-E_m)}$$

$$\times\,\theta(|E_n-E_m-\tilde{\omega}_j|-\Delta\omega). \tag{11}$$

The regularization parameter $\Delta\omega$ can be set to zero if only excitations at $\tilde{\omega}_j$ are present [define $\theta(0)=0$]. For Heisenberg chains at intermediate temperatures and frequencies a choice of $\Delta\omega=0.1J$ yields reliable results. For higher frequencies the results for the real part of the correlation functions are free of finite-size effects.

B. Field-theoretical preliminaries and transformations

The correlations described by $\chi(q,\omega)$ Eq. (2) are dominant at $q=\pi$ reflecting the antiferromagnetic instability of the system. We will thus focus on this wave vector. For $q\sim\pi$ and $J_2=0$ the spin-correlation function has been studied in detail with bosonization techniques by Schulz[12] and has later been improved including logarithmic corrections.[18] The result of conformal-field theory for any two-point function with scaling dimension x in Euclidean space (r,τ) at low temperature T is[13]

$$\chi_{\mathrm{CFT}}(r,\tau)=\chi_0\left[\frac{\frac{\pi T}{v}}{\sinh\pi T\left(\frac{r}{v}+i\tau\right)}\,\frac{\frac{\pi T}{v}}{\sinh\pi T\left(\frac{r}{v}-i\tau\right)}\right]^x, \tag{12}$$

where v denotes the velocity of the low-lying spin excitations, and χ_0 is some constant. The spin-wave velocity for frustrated Heisenberg chains has been determined numerically as $v=0.5\pi(1-1.12J_2)$ for $J_2<0.2411$.[27–29] The Fourier representation in momentum q and frequency ω space with $\mathrm{Im}\,\omega>0$ is

$$\chi_{\mathrm{CFT}}(q,\omega)=\sin(\pi x)v^{1-2x}\chi_0(\pi T)^{2x-2}$$

$$\times F_x\left(\frac{\omega-v(q-\pi)}{2\pi T}\right)F_x\left(\frac{\omega+v(q-\pi)}{2\pi T}\right) \tag{13}$$

with

$$F_x(k)=\int_0^\infty d\lambda\,\frac{e^{i\lambda k}}{(\sinh\lambda)^x}$$

$$=2^{x-1}\Gamma(1-x)\frac{\Gamma(x/2-ik/2)}{\Gamma(1-x/2-ik/2)}. \tag{14}$$

The value of the scaling dimension x depends on the strength of the interaction or the anisotropy in case of a spin chain. For the XY model we have $x=1$ and for the isotropic Heisenberg chain $x=1/2$. In the lower half plane $\chi_{\mathrm{CFT}}(q,\omega)$ is given by Eq. (13) with ω replaced by $-\omega$.

From this representation we learn that the function on the right-hand side of Eq. (13) is analytic in a strip around the real axis with $|\mathrm{Im}\,\omega|<x2\pi T$ as long as $T>0$; for $T=0$ we have

$$\mathrm{Im}\,\chi_{\mathrm{CFT}}(q,\omega)\simeq\begin{cases}0 & \text{for } \omega<v|q-\pi|\\ [\omega^2-v^2(q-\pi)^2]^{x-1} & \text{else.}\end{cases} \tag{15}$$

These analytical properties are shared by the structure factor $S_{\mathrm{CFT}}(q,\omega)$, which is related to $\mathrm{Im}\,\chi_{\mathrm{CFT}}(q,\omega)$ via Eq. (3), i.e., it is analytic in $|\mathrm{Im}\,\omega|<x2\pi T$ for $T>0$, and $S_{\mathrm{CFT}}(\pi,\omega)\simeq\omega^{2x-2}$ for $T=0$.

Performing the Fourier transform to real time we see that both $\chi_{\mathrm{CFT}}(q,t)$ and $S_{\mathrm{CFT}}(q,t)$ decay exponentially at finite temperatures and algebraically for $T=0$ and $q=\pi$,

$$\chi_{\mathrm{CFT}}(\pi,t)\simeq\begin{cases}\exp(-x2\pi Tt) & \text{for } T>0\\ t^{1-2x} & \text{for } T=0.\end{cases} \tag{16}$$

For momenta $q\neq\pi$ the function $\chi_{\mathrm{CFT}}(q,t)$ decays exponentially with time t for any $T>0$ as well as $T=0$.

There are additional contributions to $\chi(q,\omega)$ and $S(q,\omega)$ on the lattice that are singular at finite values of ω even for $T>0$. These contributions have their origin in the existence of the lattice that leads to finite-energy bands with upper-band-edge singularities. There are no universal predictions like for the lower band edge governed by conformal-field theory and described above. An exception, of course, is the XY spin model that can be mapped to free fermions.

As we discuss in Sec. I C the case of the XY model suggests to assume that $\chi(q,\omega)$ is singular at a frequency Λ where the imaginary part diverges like

$$\mathrm{Im}\,\chi(q,\omega\pm i\epsilon)=\begin{cases}\pm(\Lambda-\omega)^{\alpha} & \text{for } \omega<\Lambda\\ 0 & \text{for } \omega>\Lambda.\end{cases} \tag{17}$$

The upper (lower) sign yields the retarded (advanced) correlation function. If not stated explicitly we discuss the retarded functions. The Kramers-Kronig transform yields the singularity of the real part

$$\mathrm{Re}\,\chi(q,\omega)=\begin{cases}\cot\pi\alpha(\Lambda-\omega)^{\alpha} & \text{for } \omega<\Lambda\\ \dfrac{1}{\sin\pi\alpha}(\omega-\Lambda)^{\alpha} & \text{for } \omega>\Lambda.\end{cases} \tag{18}$$

In the neighborhood of $\alpha=0$ we have a logarithmic singularity[21]

$$\mathrm{Re}\,\chi(q,\omega)=\frac{1}{\pi}\ln|\Lambda-\omega|. \tag{19}$$

Regarding the time dependence we note that both functions $\chi(q,t)$ and $S(q,t)$ are dominated by the singularity at Λ and show long-time asymptotics

$$\chi(q,t)\simeq t^{-(1+\alpha)}\exp(-i\Lambda t). \tag{20}$$

Since the operator S^z is self-adjoint $\mathrm{Im}\,\chi(\pi,\omega)$ is odd in ω. In general we thus set $\mathrm{Im}\,\chi(q,\omega)\sim\mathrm{sgn}(\omega)(\Lambda^2-\omega^2)^{\alpha}$. The Fourier transform (FT) of $\chi(\pi,\omega)$ is consequently identical to twice the sine transform of $\mathrm{Im}\,\chi(\pi,\omega)$ and $\chi(\pi,t)$ is real. For the XY case with $\alpha=-1/2$ we like to note more explicitly the qualitative result

$$\mathrm{Im}\,\chi(\omega\pm i\epsilon)=\begin{cases}\pm\dfrac{\mathrm{sgn}(\omega)}{\sqrt{\Lambda^2-\omega^2}} & \text{for } |\omega|<\Lambda\\ 0 & \text{for } |\omega|>\Lambda,\end{cases} \tag{21}$$

with Kramers-Kronig transform

$$\mathrm{Re}\,\chi(\omega)=\begin{cases}\dfrac{2}{\pi}\dfrac{\mathrm{arcsinh}\sqrt{\left(\dfrac{\Lambda}{\omega}\right)^2-1}}{\sqrt{\Lambda^2-\omega^2}} & \text{for } |\omega|<\Lambda\\ -\dfrac{2}{\pi}\dfrac{\arcsin\sqrt{\dfrac{\Lambda}{\omega}}}{\sqrt{\omega^2-\Lambda^2}} & \text{for } |\omega|>\Lambda.\end{cases} \tag{22}$$

For overcritical frustration[15] $J_2>J_c=0.2411$ the Heisenberg chain exhibits a gapped spectrum with a lower bound Ω_g. Considering square-root divergences at the lower and upper edge of the spectrum

$$\mathrm{Im}\,\chi(\omega\pm i\epsilon)=\begin{cases}\pm\dfrac{\mathrm{sgn}(\omega)}{\sqrt{(\omega^2-\Omega_g^2)(\Lambda^2-\omega^2)}} & \text{for } \Omega_g<|\omega|<\Lambda\\ 0 & \text{else,}\end{cases} \tag{23}$$

we obtain the Kramers-Kronig transform

$$\mathrm{Re}\,\chi(\omega)=\begin{cases}0 & \text{for } \Omega_g<|\omega|<\Lambda,\\ \pm\dfrac{\mathrm{sgn}(\omega)}{\sqrt{(\omega^2-\Omega_g^2)(\omega^2-\Lambda^2)}} & \text{else.}\end{cases} \tag{24}$$

The upper-band-edge singularities and the resulting algebraic real-time asymptotics exist only at sufficiently low temperatures. At intermediate temperatures the upper limit of the continuum yields an antisymmetrized Lorentzian contribution.

$$\mathrm{Im}\,\chi(q,\omega)\simeq L_-(\phi)-L_+(\phi), \tag{25}$$

where

$$L_{\pm}(\phi)=\frac{\Gamma\cos\phi-(\Lambda\pm\omega)|\sin\phi|}{\Gamma^2+(\Lambda\pm\omega)^2}. \tag{26}$$

Limiting $0\leqslant\phi\leqslant\pi/2$ the real part is simply given by

$$\mathrm{Re}\,\chi(q,\omega)\simeq L_-(\phi-\pi/2)+L_+(\phi-\pi/2) \tag{27}$$

and the Fourier transform reads

$$\chi(q,\omega)\simeq e^{-\Gamma t}\sin(\Lambda t+\phi). \tag{28}$$

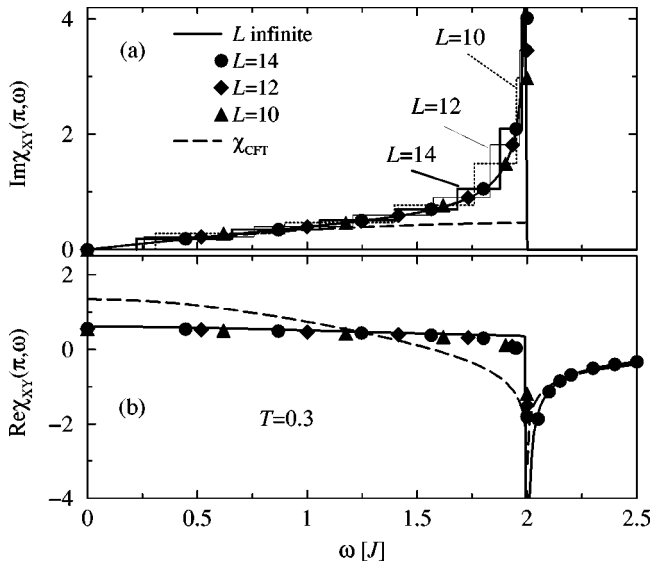

FIG. 1. Susceptibility for the XY model: (a) imaginary part, (b) real part. The full line in (a) is the exact results from Eq. (29), the symbols are obtained via Eq. (10), and the step functions via Eq. (9). The dashed line is the result from field theory with upper-band-edge cutoff but without divergence. The lines in (b) are the Kramers-Kronig transforms of the imaginary part, and the symbols are obtained using Eq. (11) with $\Delta\omega=0$.

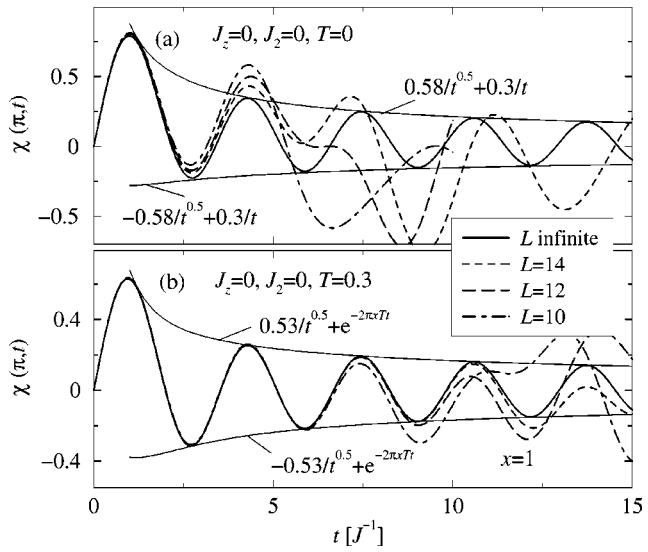

FIG. 2. Real-time spin-correlation function in the XY case at $T=0$ (a) and $T=0.3$ (b). Thermodynamic limit results (full lines) are obtained via Eq. (30). The different broken lines show the deviation of results for finite systems from Eq. (8). $L=14$ yields a good representation of the correlation function up to $t\approx 2/J$ at $T=0$ and up to $t\approx 8/J$ at $T=0.3$. The thin lines show the asymptotic behavior as predicted in Sec. I B.

This temperature range will be referred to as ''diffusive regime.''

C. XY model

We demonstrate the overlap of the accurate short-time-scale results from the exact diagonalization of finite systems and the asymptotic behavior accessible by field theory for an exactly solvable case, the XY model, where $J_2=J_z=0$. The spin operators in this model can be transformed to non-interacting, spinless fermions via a Jordan-Wigner transformation.[30] The structure factor Eq. (3) can be given for $L\to\infty$ in closed form.[8] The imaginary part of the susceptibility at $q=\pi$ is

$$\mathrm{Im}\,\chi_{XY}(\pi,\omega)=\tanh(\beta\omega/4)(4-\omega^2)^{-0.5}. \tag{29}$$

This is the field-theoretical result Eq. (13) with scaling dimension $x=1$ multiplied with the square-root divergence at the upper band edge. The limit of $T\to 0$ is given by Eqs. (21) and (22).

Figure 1(a) shows the imaginary part of the susceptibility. The full line represents the exact results, the symbols are obtained via the regularization Eq. (10), and the step functions are given by Eq. (9). The dashed line is the result from field theory with an UV cutoff but without the upper-band-edge divergence. Figure 1(b) shows the real part, the lines are the Kramers-Kronig transforms of the imaginary part and the symbols are obtained using Eq. (11) with $\Delta\omega=0$.

We conclude that the multiplicative approach of the low-energy description from field theory with the high-energy behavior is adequate. Also, the numerical approaches give a reasonable approximation to the exact result. The values of the real part for $\omega>\Lambda$ show only very little finite-size effects. The divergences of the real and the imaginary part at the upper band edge show the correspondence predicted by Eqs. (21) and (22).

The retarded, real-time correlation function can be determined numerically in the thermodynamic limit

$$\chi(q,t)=i\,\theta(t)\lim_{L\to\infty}\frac{1}{L}\sum_k\,(f_k-f_{k+q})\exp[i(E_k-E_{k+q})t]. \tag{30}$$

The energy dispersion is given by $E_k=J\cos k$, f_k are Fermi distribution functions, and the sum covers the first Brillouin zone. In general for $L\geqslant 10^4$ the result is independent of L for all practical purposes.

In Fig. 2 we show the retarded spin-correlation function for finite systems compared with the result in the thermodynamic limit ($L\to\infty$, full lines) at $T=0$ (a) and at $T=0.3$ (b). The different broken lines show the deviation of results for finite systems Eq. (8). $L=14$ yields a good representation of the correlation function up to $t\approx 2/J$ at $T=0$ and up to $t\approx 8/J$ at $T=0.3$.

The thin solid lines in Fig. 2 show the asymptotic $t^{-0.5}$ behavior from the upper-band-edge divergence. The contribution from the low frequencies yields an additive term $\sim t^{-1}$ at $T=0$ and $\sim e^{-x2\pi Tt}$ with $x=1$ at $T=0.3$ as predicted in Sec. I B. The fits have been obtained for $80<tJ<100$ to assure the asymptotic limit. The numerical data for finite systems and for $T\approx 0.3$ yield a good representation of the correlation function in the thermodynamic limit up to time scales that are already dominated by the asymptotic, large-time-scale behavior.

D. Technical outline of the approach

Renormalization-group studies show that the XY model is one point of the line of critical fixed points towards which the interaction flows in a bosonized representation of the Heisenberg model ($J_z=1$).[31,32] One thus expects qualitatively similar results for the unfrustrated Heisenberg chain as in the XY model. This should also hold for frustrated Heisenberg chains, at least for under-critical $J_2 \leqslant J_c = 0.2411$.[14,32,15]

The discussion of the XY model implies that the representation of the imaginary part of the correlation function is best achieved by multiplying the upper-band-edge behavior to the field-theoretical expression,

$$\mathrm{Im}\,\chi(\pi,\omega) = \mathrm{Im}[\chi_{\mathrm{CFT}}(\pi,\omega)] \frac{(\Lambda^2-\omega^2)^\alpha}{2\Lambda^{2\alpha}} \theta(\Lambda-|\omega|). \tag{31}$$

The real part of the susceptibility is given by the numerical Kramers-Kronig transform (KKT) of Eq. (31). The real-time representation is obtained by FT of $\chi(\pi,\omega)$. We attempt this approach for frustrated Heisenberg chains and at finite temperatures, where the exact form of the correlation function is not known.

The field-theoretical expression in Eq. (31) depends on the parameter of the scaling dimension x and a global prefactor $v^{1-2x}\chi_0$. The latter is determined by requesting the sum rule of the first moment of the susceptibility to be correctly reproduced. The sum rule

$$I_1(q,T) = \frac{1}{\pi}\int_{-\infty}^{\infty} d\omega\, \omega\, \mathrm{Im}\,\chi(q,\omega) \tag{32}$$

can be extracted very accurately from the finite-size data as discussed in Sec. II. We are then left with the parameter vector $\mathbf{p}(T)=[x,\Lambda,\alpha]$ that we find to be temperature dependent. The scaling variable x determines the low-frequency behavior of the imaginary and the real part of the susceptibility [Eq. (15)] as well as the decay in real-time space as given by Eq. (16). The upper continuum edge Λ positions the cusp or divergence of the real part [Eq. (18)] as well as the oscillatory behavior of $\chi(\pi,t)$ as a function of time [Eq. (20)]. Finally the exponent α describes the shape of the real-part cusp or divergence [Eq. (18)] and the decay of the oscillations in time [Eq. (20)].

II. SUM RULES AND PREFACTORS

Since the imaginary and real representation of the spin-correlation function are Kramers-Kronig related and as a consequence of the bounded excitation spectrum[33] it is straightforward to find that the sum-rule Eq. (32) is given by

$$I_1(q,T) = -\lim_{\omega\to\infty} \omega^2 \mathrm{Re}\,\chi(q,\omega). \tag{33}$$

For $\lim_{T\to 0} I_1(q,T) = 4K_1(q)$ the structure-factor sum rule discussed in Ref. 17 is reproduced. For arbitrary frustration J_2 the structure-factor sum rules are connected to the ground-state energy E_G of the system via $K_1(\pi)/2 + K_1(0.5\pi) = 2E_G/3$. We recall that for $J_2=0$ and $J_2=0.5$ one has $K_1(q) = 2(1-\cos q)E_G/3$. For $J_2=0.5$ the average $\langle S^z_l S^z_{l+2}\rangle_{T=0} = 0$ vanishes.[34]

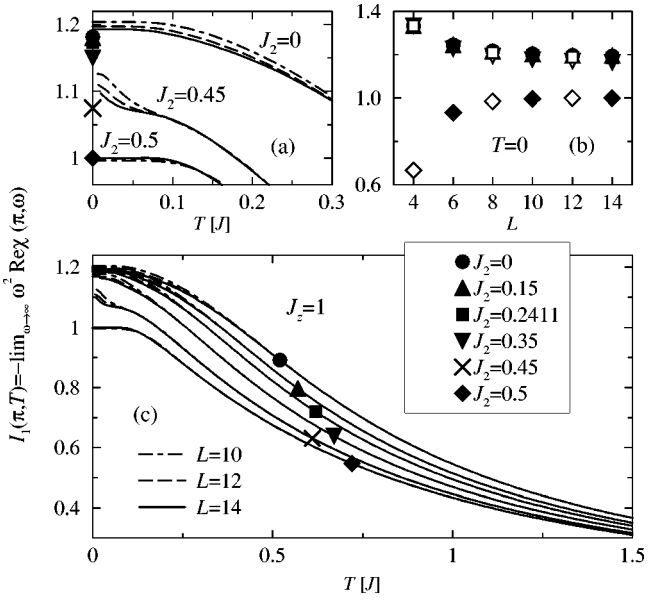

FIG. 3. First moment of the spin susceptibility as extracted from the asymptotics of the real part in finite systems. (a) Low-temperature finite-size effects and thermodynamic limit values as extracted from the finite size scaling represented in (b). (c) Temperature dependence.

The crucial point is that $\mathrm{Re}\,\chi(q,\omega\to\infty)$ depends only weakly on the system size L.[21] Figure 3(c) shows $I_1(q,T)$ as a function of temperature for different system sizes and frustration parameters. In Fig. 3(a) it becomes obvious that the result for $J_2=0$ and $L=14$ is for all practical purposes in the thermodynamic limit for $T>0.3$. Analyzing Eq. (12) one finds the correlation length to be $\xi = v/(2\pi x T)$. For $x\sim 0.5$ and $v = 0.5\pi(1-1.12J_2)$ we find that the finite-size effects are of the order of 10^{-3} when the correlation length becomes $\xi \sim L$.

Figure 3(b) shows the values of $I_1(\pi,0)$ as a function of the system size. We determine the thermodynamic limit with the algebraic scaling function $I_1(\pi,0,L) = I_1(\pi,0,\infty) + A_0 L^{-\eta}$. Systems with $L \bmod 4 = 0$ [open symbols in Fig. 3(b)] in general converge differently than systems with $L \bmod 4 = 2$ (full symbols). The two cases yield two values the difference of which serves as an error estimate. For $J_2=0$ we find $I_1(\pi,0,\infty) = 1.1821(7)$ that is very close to the exact value of $I_1(\pi,0) = 1.181\,725\,8\ldots$. For $J_2=0.15$ and $J_2=0.2411$ we find $I_1(\pi,0) = 1.185(10)$ and $I_1(\pi,0) = 1.173(2)$, respectively. A value of $I_1(\pi,0) = 1.1521(5)$ has been found for $J_2=0.35$. The result for $J_2=0.5$ with $I_1(\pi,0) = 1.000(3)$ is extremely close to the exact value of 1. In Fig. 3(a) the peculiar finite-size effects for $J_2=0.45$ become apparent. Obviously they result from the gap value[15] of $\Omega_g \approx 0.12$ being just in the temperature range where the finite-size effects appear. The determination of $I_1(\pi,0) = 1.075(10)$ is thus less accurate. The results are represented by the symbols in Fig. 3(a).

In Fig. 3(c) the temperature dependence of $I_1(\pi,T)$ is

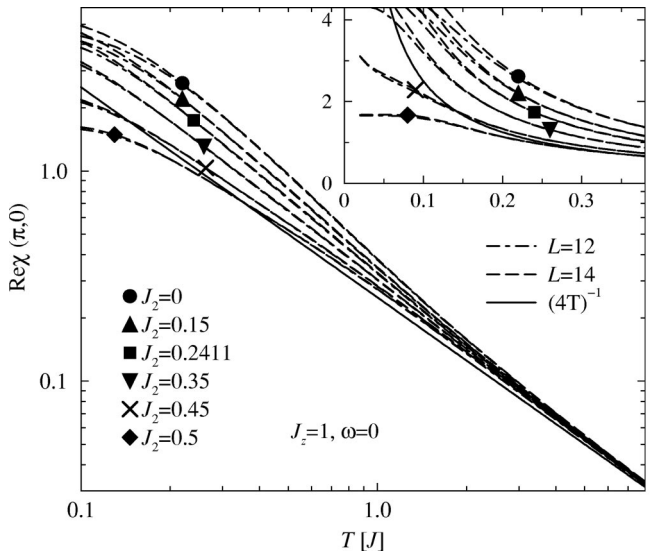

FIG. 4. Log-Log plot of Re $\chi(\pi,\omega=0)$ from Eq. (6) as a function of temperature. The full line is the universal large T asymptotic result $\sim 0.25/T$. The inset shows the finite-size effects at low temperatures. $\lim_{T\to 0}$Re $\chi(\pi,\omega=0)$ diverges for $J_2 \leqslant 0.2411$ and saturates for $J_2 > 0.2411$.

shown for different values of the frustration parameter. The general asymptotic behavior of $\lim_{T\to\infty}\chi(\pi,\omega)\sim T^{-1}$ becomes apparent from the discussion in Sec. III F. For the first moment we find $\lim_{T\to\infty} I_1(\pi,T)=0.5/T$. This is reminiscent of the structure-factor sum rule

$$-\lim_{\substack{T\to\infty\\ \omega\to\infty}} T\omega^2 \mathrm{Re}\,\chi(\pi,\omega)=\lim_{T\to\infty}\int_{-\infty}^{\infty} d\omega'\,\omega'^2 S(\pi,\omega')=0.5 \tag{34}$$

and is generic for all values of J_2 and the XY model. Note that $\lim_{T\to\infty} S(q,\omega)=\lim_{T\to\infty} S(q,-\omega)$.

The values of Re $\chi(\pi,\omega=0)$ show little finite-size effects even at rather low temperatures. Figure 4 shows a log-log plot from Eq. (6) for different values of the frustration J_2 and chain lengths as a function of temperature (broken lines). The full line shows the asymptotic behavior

$$-\lim_{T\to\infty} T\mathrm{Re}\,\chi(\pi,0)=\lim_{T\to\infty}\int_{-\infty}^{\infty} d\omega' \;\; S(\pi,\omega')=0.25, \tag{35}$$

which reproduces a structure-factor sum rule and is identical for all values of the frustration and the XY model. The field-theoretical prediction Eq. (13) for the prefactor T^{2x-2} with constant scaling variable x is clearly inappropriate for the temperature range shown. Our analysis in Sec. III shows that the deviation results from an explicit temperature dependence of the $x(T)$ as well as from the temperature dependence of the singularity at the upper band edge, i.e., $\Lambda(T)$ and $\alpha(T)$.

The inset of Fig. 4 shows the finite-size effects at low temperatures. $\lim_{T\to 0}$Re $\chi(\pi,\omega=0)$ diverges for $J_2 \leqslant 0.2411$ and saturates for $J_2 > 0.2411$ which is reminiscent of the presence of a gap.[15]

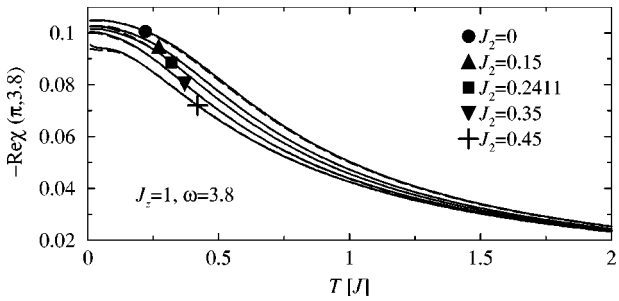

FIG. 5. Temperature dependence of Re $\chi(\pi,3.8)$ from Eq. (6). The finite-size effects are $\leqslant 0.1\%$ and hardly visible on this scale (full lines $L=14$, broken lines $L=12$).

For completeness we show in Fig. 5 the temperature dependence of Re $\chi(\pi,3.8)$ from Eq. (6) for different values of J_2. The finite-size effects are $\leqslant 0.1\%$ and hardly visible on this scale (full lines $L=14$, broken lines $L=12$). We do not show plots for $J_2=0.5$ since the presence of bound states makes the result unreliable, cf. Sec. III C.

III. FRUSTRATED HEISENBERG CHAINS

We now turn to the determination of lineshapes of the spin-correlation function in frustrated Heisenberg chains making use of the precise results obtained above.

A. Critical frustration

We first discuss the values of $J_z=1$ and $J_2=J_c$ at the quantum-critical point making the field-theoretical results eligible for comparison. In frequency space at $T=0$ for a 14-site chain there are four spectral lines at frequencies $\tilde{\omega}_j \in \mathcal{W}^{(14)}_{.2411}=\{0.264,1.309,2.112,2.437\}$ which, by analogy to the dimer-dimer correlation functions,[21] may be identified as the triplet excitations out of the ground state.[35] It is thus reasonable to suppose them to form a well-defined continuum in the thermodynamic limit and thus Eqs. (10) and (11) can be applied with $\Delta\omega=0$.

The imaginary part of the spin-correlation function is shown in Fig. 6(a). The bins are obtained using Eq. (9) and the symbols are given using Eq. (10). The symbols in Fig. 6(b) show the real part as given by Eq. (11). For $\omega=0$ finite-size effects are significant since one expects from field theory and by analogy to the XY model Re $\chi^{(T=0)}(\pi,\omega=0)\to\infty$. For $\omega>3$ the numerical results are essentially in the thermodynamic limit as can be seen from the different broken lines in the inset of Fig. 6(b). The real-time representation of the spin-correlation function at $T=0$ is given in Fig. 7(a). As in the XY case the system with $L=14$ yields a useful representation of the correlation function up to $t \approx 2/J$.

The fit with the theoretical predictions from Eq. (31), its KKT, and FT are given by the full lines in Figs. 6(a), 6(b), and 7(a) using the parameter set $\mathbf{p}_{0.2411}(0)=[0.50(1),2.6(1),-0.10(7)]$. The cutoff $2.5<\Lambda$ is bound by the highest spectral lines that must lie in the continuum. Previous results[5] suggest Λ to decrease monotonously with frustration and for reasons of consistency $\Lambda<2.7$. The

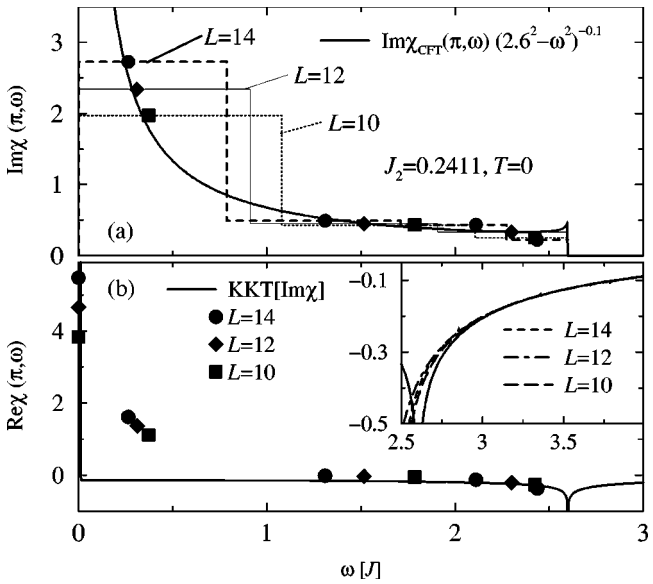

FIG. 6. Imaginary part (a) and real part (b) of the spin-correlation function in the frustrated Heisenberg chain at $T=0$ with $J_2=0.2411$. The imaginary part for finite systems is binned [Eq. (9)], each bin holds one spectral line, symbols are from Eq. (10). The symbols for the real part are obtained by using Eq. (11). The full lines are the theoretical result from Eq. (31) and its KKT. Inset: enlargement of cutoff region with finite-size results from Eq. (6).

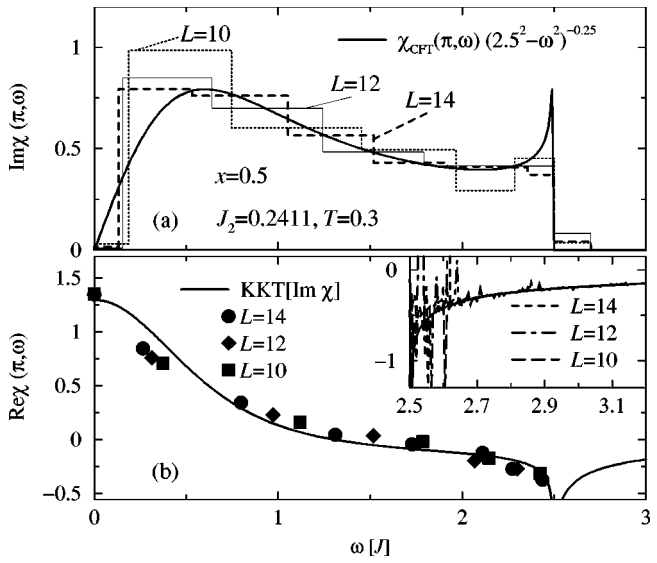

FIG. 8. Imaginary part (a) and real part (b) of the spin-correlation function in the frustrated Heisenberg chain at $T=0.3$ with $J_2=0.2411$. The imaginary part for finite systems is binned [Eq. (9)], the symbols for the real part are obtained using Eq. (11). The full lines are the theoretical result from Eq. (31) and its KKT. Inset: enlargement of cutoff region with finite-size results from Eq. (6).

three parameters are then determined by matching the first maximum as well as the slope for $1<tJ<2$ in the real-time representation and the value of the real part for $\omega\sim 3.8$ [cf. Fig. (5)]. The finite-size effects require us to allow for rather large error margins.

The result of x is consistent with the prediction from field theory. The value of $\alpha\neq 0$ suggests a more complicated upper continuum edge than a simple ultraviolet cutoff. We emphasize that the overall prefactor of the fit function is fixed by the sum rule Eq. (32) and that values for Λ and α have been obtained without using the not-so-well-defined binned data of the imaginary part.

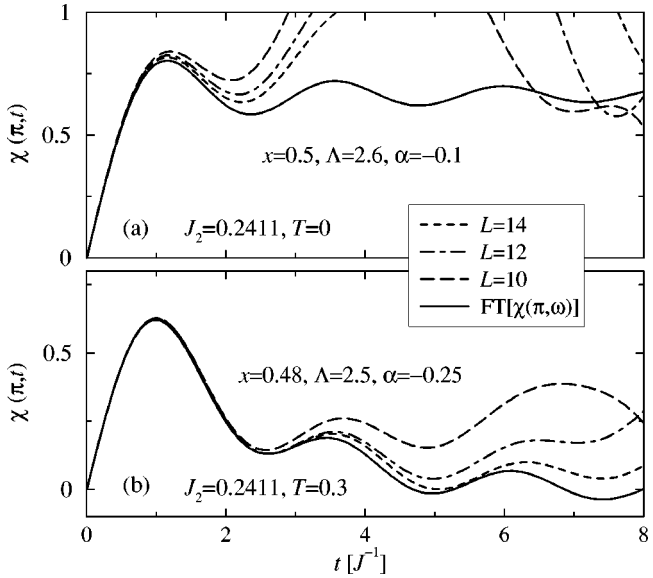

FIG. 7. Real-time spin-correlation function for $J_2=0.2411$ at (a) $T=0$ and (b) $T=0.3$. Broken lines are finite-size data from Eq. (8), full lines are FT of Eq. (31).

The plot of the real-time representation of the spin-correlation function at $T=0.3$ in Fig. 7(b) reveals the temperature dependence of the parameter vector $\mathbf{p}_{0.2411}(0.3)=[0.48(1),2.5(1),-0.25(5)]$. The result for $L=14$ yields a useful representation of the correlation function up to $t\approx 4/J$. The full line is the fit from the FT of Eq. (31). The exponential fall off predicted in Sec. I B is confirmed and renders the value of the scaling dimension. The oscillations are much less damped than would be obtained with an upper-band-edge exponent of $\alpha=0$ thus yielding the negative value of $\alpha=-0.25$. The cutoff Λ is given via the period of the oscillations.

Figures 8(a) and 8(b) show the imaginary and real part of the frequency representation of the spin-correlation function at $T=0.3$, respectively. The binned data for the imaginary part via Eq. (9) and the symbols for the real part via Eq. (11) are obtained for the sets of dominant spectral lines, in the case of $L=14$ they are given by the frequencies $\tilde{\omega}_j \in \tilde{\mathcal{W}}^{(14)}_{.2411}=\{0.311,0.971,1.517,2.068,2.301\}$. The condition of a well-defined continuum with respect to Bethe ansatz quantum numbers is violated and thus Eq. (10) cannot be applied any more. For the real part the data are regularized with $\Delta\omega=0.1$, which is determined to give reliable results analogously to the dimer-dimer correlation functions.[21] An exception is made at $\omega=0$, where no regularization is applied $(\Delta\omega=0)$.

The good correspondence of the field-theoretical fits from Eq. (31) and its KKT (solid lines) in Figs. 8(a) and 8(b)

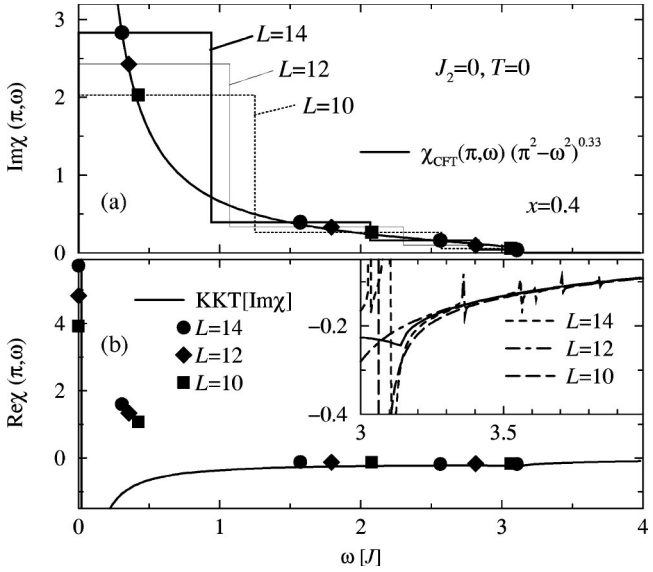

FIG. 9. Imaginary part (a) and real part (b) of the spin-correlation function in the unfrustrated Heisenberg chain at $T=0$. The binned curves in (a) are from [Eq. (9)], the symbols are from Eq. (10). The symbols for the real part (b) are obtained using Eq. (11). The full lines are the fits from Eq. (31) and its KKT. Inset: enlargement of cutoff region with finite-size results from Eq. (6).

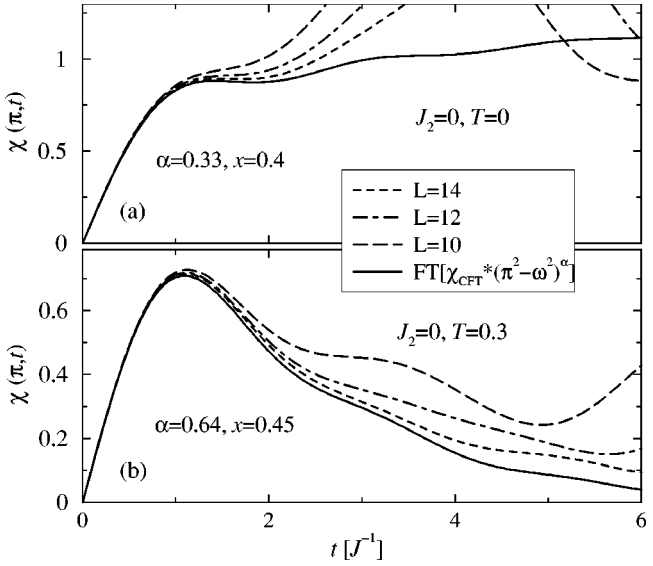

FIG. 10. Real-time spin-correlation function for $J_2=0$ at (a) $T=0$ and (b) $T=0.3$. Broken lines are finite-size data from Eq. (8), full lines are FT of Eq. (31).

proves the reliability of the parameters extracted from the real-time representation. Especially the good agreement of the values of $\mathrm{Re}\,\chi(\pi,0)$ and of $\mathrm{Re}\,\chi(\pi,\omega>2.7)$ [inset Fig. 8(b)] are nontrivial consistency checks. We expect a thermal smearing out of the small divergence at the upper band edge of which the shape is not known and that we did not account for [solid line in Fig. 8(a)]. This might have a small influence on the parameters extracted and thus we adapted rather conservative error bars. The finite-size data in both the real and imaginary part suggest a steeper slope in the low-frequency dependence of the fitted curves. Together with the temperature dependence of the scaling dimension x this indicates the breakdown of the scale invariance predicted by field theory at finite temperatures.[36]

B. Unfrustrated Heisenberg chain

Heisenberg chains without frustration are relevant for most of the magnetically quasi-one-dimensional systems studied experimentally. Since the system is integrable the numerical data can be compared to results from Bethe ansatz.

At $T=0$ the four spectral lines of the triplet excitations out of the ground state for a 14-site chain are at frequencies $\tilde{\omega}_j \in \mathcal{W}_0^{(14)}=\{0.307,1.57,2.56,3.10\}$.[1,2,20] It is thus reasonable to suppose them to form a well-defined continuum in the thermodynamic limit and thus Eqs. (10) and (11) can be applied with $\Delta\omega=0$. Binned data for the imaginary part are obtained via Eq. (9).

The imaginary part of the spin-correlation function is shown in Fig. 9(a). The real part in Fig. 9(b) shows for $\omega=0$ significant finite-size effects since $\mathrm{Re}\,\chi^{(T=0)}(\pi,\omega=0)\to\infty$. For $\omega>3.5$ the numerical results are essentially in the thermodynamic limit [inset of Fig. 9(b)]. The real-time representation of the spin-correlation function at $T=0$ is given in Fig. 10(a).

The upper edge of the two-spinon continuum is known exactly to be $\Lambda=\pi$.[37] Bethe ansatz results suggest that the infrared divergence of the two-spinon contribution $\chi^{(2)}$ to the imaginary part of the spin-correlation function has a logarithmic correction

$$\lim_{|\omega|\to 0} \mathrm{Im}\,\chi^{(2)}(\pi,\omega)\propto\omega^{-1}\sqrt{\ln|\omega^{-1}|}, \tag{36}$$

while at the upper continuum edge it vanishes square rootlike.[17] The two-spinon contribution has been found to contribute 72.89% to the total spectral weight.[17] Our and previous numerical studies show that the spectral weight of the total correlation function for above the two-spinon continuum ($\omega>\pi$) at $q=\pi$ is less than 0.1%.[8,5] Thus the total spin-correlation function includes also about 27% higher-order contributions and we have $\mathrm{Im}\,\chi(\pi,\omega)>\mathrm{Im}\,\chi^{(2)}(\pi,\omega)$. Consequently we must require $\alpha\leqslant 0.5$ and $\Lambda=\pi$. Using x as an effective fit parameter we also have $x\leqslant 0.5$. Note that within the numerical precision of our results, the fit procedure with parameter $x<0.5$ is consistent with an actual scaling dimension $x=0.5$ plus logarithmic corrections.

From the amplitude in the real-time representation in Fig. 10(a) we find that the parameters x and α fall on a line defined by $(0.38,0.25)<(x,\alpha)<(0.44,0.5)$. Taking also the value of the real part at $\omega=4$ in the inset of Fig. 9(b) into consideration we determine $\mathbf{p}_0(0)=[0.40(3),\pi\pm 0.01,0.33(5)]$. The error margins have been chosen rather large because of the obvious finite-size effects. The resulting fits with the theoretical predictions from Eq. (31), its KKT, and FT are given by the full lines Figs. 9(a), 9(b), and 10(a) and show satisfactory agreement with the results from finite systems.

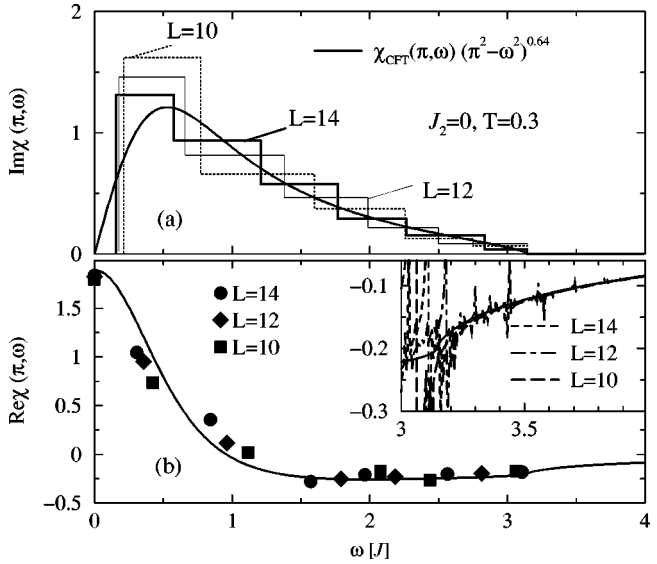

FIG. 11. Imaginary part (a) and real part (b) of the spin-correlation function in the unfrustrated Heisenberg chain at $T=0.3$. The step function in (a) is from [Eq. (9)], the symbols in (b) from Eq. (11). The full lines are from Eq. (31) and its KKT. Inset: enlargement of cutoff region with results from Eq. (6).

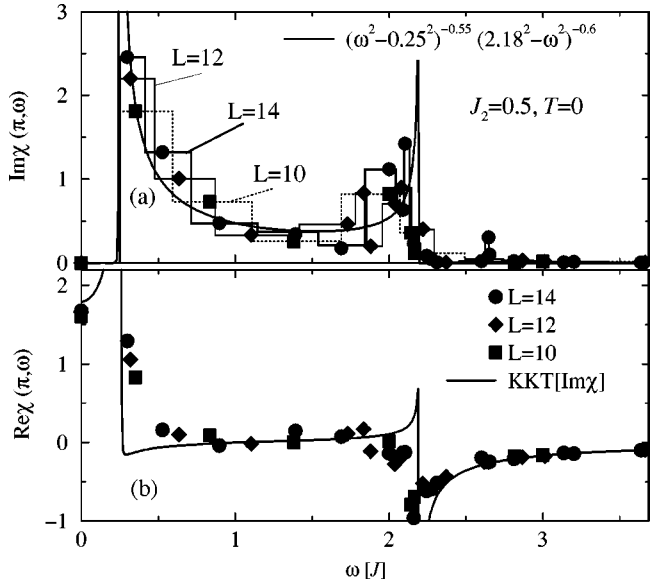

FIG. 12. Imaginary part (a) and real part (b) of the spin-correlation function for $J_2=0.5$ at $T=0$. The binned curves in (a) are from [Eq. (9)], the symbols are from Eq. (10). The symbols for the real part (b) are obtained using Eq. (11). The full lines are the fits from Eq. (31) and its KKT.

The short-dashed line in Fig. 10(b) shows the correlation function for 14 sites in the real-time representation. The exponential decay in time implies a scaling dimension of $x>0.4$ and the strongly damped oscillations an exponent $\alpha>0.5$. The real part at higher frequencies as shown in the inset of Fig. 11(b) requires the exponent to be $\alpha<0.7$. Together with a matching value for Re $\chi(\pi,\omega=0)$ the parameter set $\mathbf{p}_0(0.3)=[0.45(2),\pi\pm0.1,0.64(10)]$ yields the best fits from Eq. (31) as shown by the full lines in Figs. 11(a), 11(b), and 10(b). The overall agreement is satisfactory, for small frequencies the numerical data suggest a slightly altered functional dependence on the frequency than is reproduced by the field-theoretical fit.[36]

C. Overcritical frustration

In the case of overcritical frustration the spectrum of the spin chains acquires a gap Ω_g.[34,15] We discuss here the value of $J_2=0.5$ for better comparability with results from literature.[34,38,39] For a two-particle (spinon) continuum one expects a density of states that diverges square rootlike both at the lower as well as at the upper edge. Previous numerical[5] and variational[39] results suggest sharp maxima in the density of states just above the lower edge Ω_g and just below the upper edge Λ of the continuum accompanied by a square rootlike vanishing at both edges. This can be understood in connection with bound states being present close to the edge of the continuum.[16]

At $T=0$ there are more spectral lines present than in the case of critical and undercritical frustration. Some of them are signatures of the bound states present in the system.[39] We still apply Eqs. (10) and (9) to extract the imaginary part of the spin-correlation function as shown in Fig. 12(a). The fluctuations of the results at the upper band edge are reminiscent of the fact that the bound states do not form a continuum in the thermodynamic limit. We do not attempt to refine the plot by extracting the bound-state contributions since results of the real part and especially the real-time representation are more reliable anyway.

Figure 12(b) shows the real part from Eq. (11) with $\Delta\omega=0.1$ for $1.5<\omega<2.3$ and $\Delta\omega=0.001$ else. The real-time representation of the spin-correlation function at $T=0$ is given in Fig. 13(a).

In order to adapt Eq. (31) to the gapped spectrum we have to include the value of the gap energy into the functions F_x in the field-theoretical expression Eq. (13) as

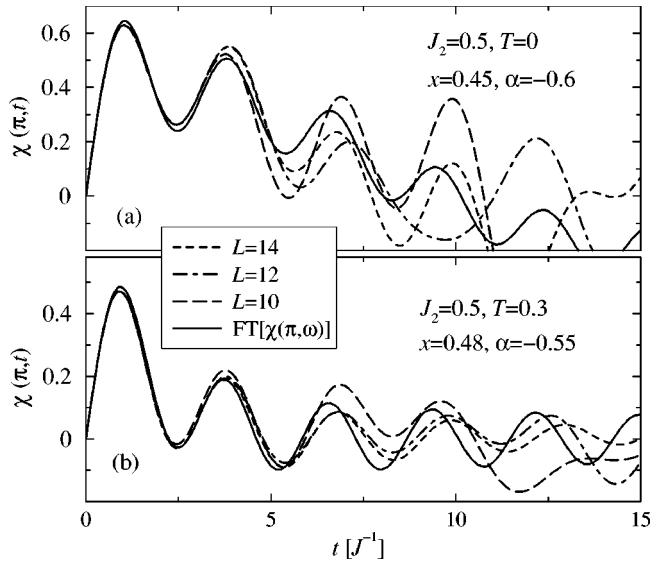

FIG. 13. Real-time spin-correlation function for $J_2=0.5$ at (a) $T=0$ and (b) $T=0.3$. Broken lines are finite-size data from Eq. (8), full lines are FT of Eq. (31).

$$F_x\left(\frac{\omega \pm v(q-\pi)}{2\pi T}\right) \rightarrow F_x\left(\frac{\omega \pm \sqrt{\Omega_g^2 + v^2(q-\pi)^2}}{2\pi T}\right). \quad (37)$$

At $T=0$ this yields the predicted divergence at the lower band edge $\mathrm{Im}\,\chi(\pi,\omega) \sim [\omega^2 - \Omega_g^2]^{x-1}$, cf. Eq. (15), while for finite temperatures $\mathrm{Im}\,\chi(\pi,\omega) \sim \omega$.

The full line in Fig. 13(a) shows the fit from the FT of Eq. (31) with $x=0.45(3)$, $\Omega_g=0.25$,[38] $\Lambda=2.18(10)$, and $\alpha=-0.6(1)$. The slow damping of the oscillations requires the large value of $|\alpha|$, there is a small frequency modulation stemming from the lower boundary Ω_g. The agreement with the finite-size data (broken lines) for the finite-size effect free time domain $tJ<5$ is not nearly as good as for the cases of lower frustration. We conclude that the simple functional form of Eq. (31) is insufficient even with the included gap via Eq. (37). The square-root dependence reported in literature[39] must be included. A perturbative examination for small J_z and J_2 shows[16] the strong interplay between the spinon continuum and bound states. Since a theoretical expression for the correct spectral weight distribution is not known we limit ourselves here to the observation that the small damping of the oscillations in Fig. 13(a) requires a rather sharp increase in $\mathrm{Im}\,\chi(\pi,\omega \rightarrow \Lambda)$.

The full lines in Figs. 12(a) and 12(b) show the fit of Eq. (31) and its KKT to the imaginary-part and real-part data, respectively. They are similar to the forms given by Eqs. (23) and (24) where $x=0.5$ and $\alpha=-0.5$. Here the parameters x and α have been adapted to roughly match the numerical values of $\mathrm{Re}\,\chi(\pi,0)$ and $\mathrm{Re}\,\chi(\pi,3.8)$. Especially the discrepancies of the fits at $\omega \sim \Lambda$ indicate that a more involved fit function is necessary.

Figure 13(b) shows that also at $T=0.3$ an accurate fit (full line) with the functional form of Eq. (31) to the finite-size data (broken lines) is not possible. The parameters for the approximate fit are $x=0.48$, $\Omega_g=0.25$,[38] $\Lambda=2.2$, and $\alpha=-0.55$. Correspondingly, the fits to the imaginary- and the real-part representations in Figs. 14(a) and 14(b) show inconsistencies with the numerical data.

D. Comparison with Lanczos and continued fraction results

The Lanczos approach allows for the evaluation of low-lying excitations in spin chains of much larger system sizes. The magnetic structure factor and thus the imaginary part of the dynamical spin-correlation function can then be determined via a continued fraction approach. We apply Eq. (10) to the results from Ref. 5 for chain lengths $L=14$ to $L=26$. We have selected only the dominant spectral lines identified as the two-spinon triplet excitations out of the ground state.[5]

Figure 15 shows on a log-log scale the fit functions derived in the previous sections (full lines) together with the results for $L=14$–26 (open circles) for next-nearest-neighbor interactions $J_2=0$ in panel (a), $J_2=J_c$ in panel (b), and $J_2=0.5$ in panel (c). For $J_2=0$ the overall agreement is excellent. For $J_2=J_c$ the discrepancies near $\omega \sim \Lambda$ can be attributed at least in part to finite-size effects near the singular continuum edge. For $J_2=0.5$ we find qualitative agreement with quantitative discrepancies consistent with the discussion in Sec. III C. A possible improvement of the fit

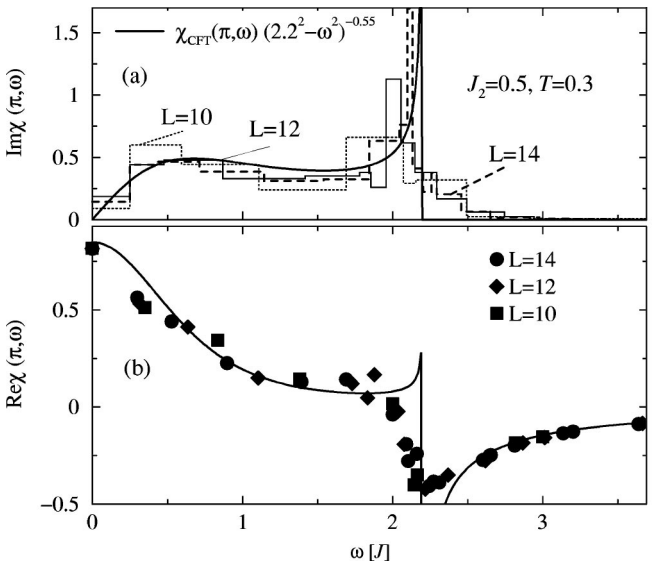

FIG. 14. Imaginary part (a) and real part (b) of the spin-correlation function for $J_2=0.5$ at $T=0.3$. The step function in (a) is from [Eq. (9)], the symbols in (b) from Eq. (11). The full lines are from Eq. (31) and its KKT.

functions at the continuum edges requires a better theoretical understanding of the interplay between bound states and the density of states at the continuum edge as discussed earlier.[16]

The overall agreement is quite satisfactory justifying both the fit parameters determined earlier and the validity of the regularization approach of Eq. (10).

E. Intermediate temperatures

At intermediate temperatures the interaction in the system is expected to broaden out all sharp features in the correla-

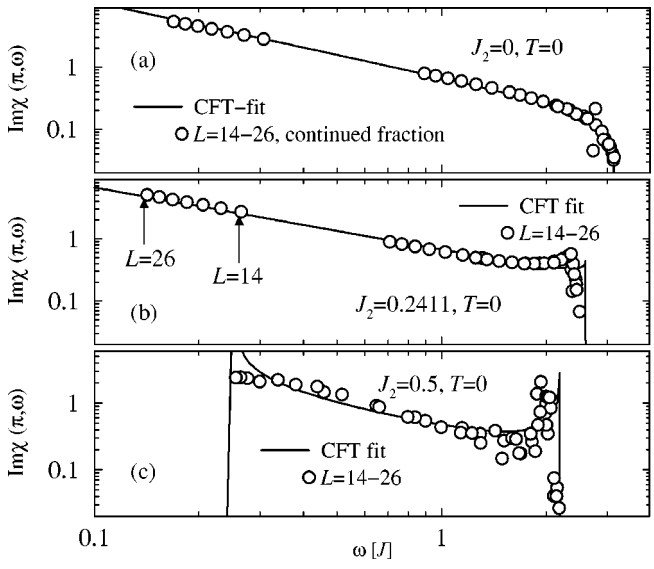

FIG. 15. Comparison of the fits from field theory (full lines) and the results obtained by applying Eq. (10) to the data for the spin correlation function from Ref. 5 (symbols) on a log-log scale. Parameters are $T=0$ and $J_2=0$ in panel (a), $J_2=0.2411$ in panel (b), and $J_2=0.5$ in panel (c).

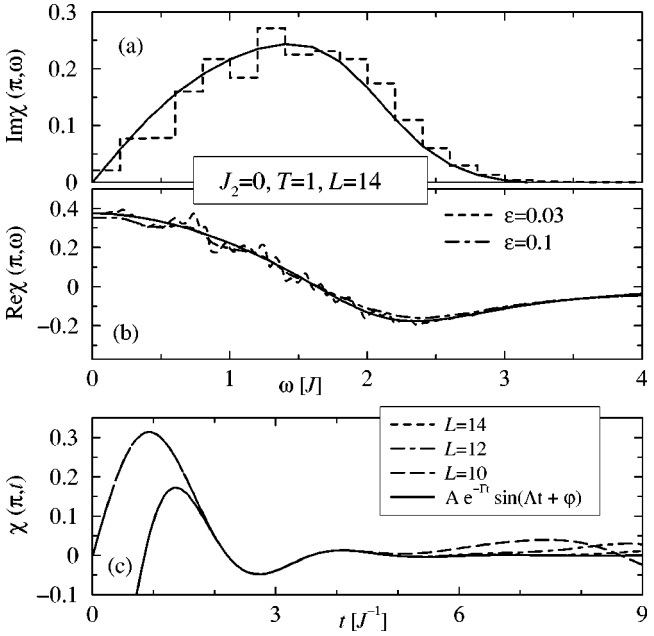

FIG. 16. Spin-correlation function of the unfrustrated Heisenberg chain at $T=1$. The broken line in (a) is the binned imaginary representation, the broken lines in (b) are the real part from Eq. (6) with two values of ϵ for regularization, all for $L=14$. Full lines in (a) and (b) are double Lorentzian fits. (c) shows the real-time representation from finite systems (broken lines) and the asymptotic fit (full line) with $\Lambda=2.31(1)$, $\Gamma=0.941(5)$, and $A=-0.67(5)$.

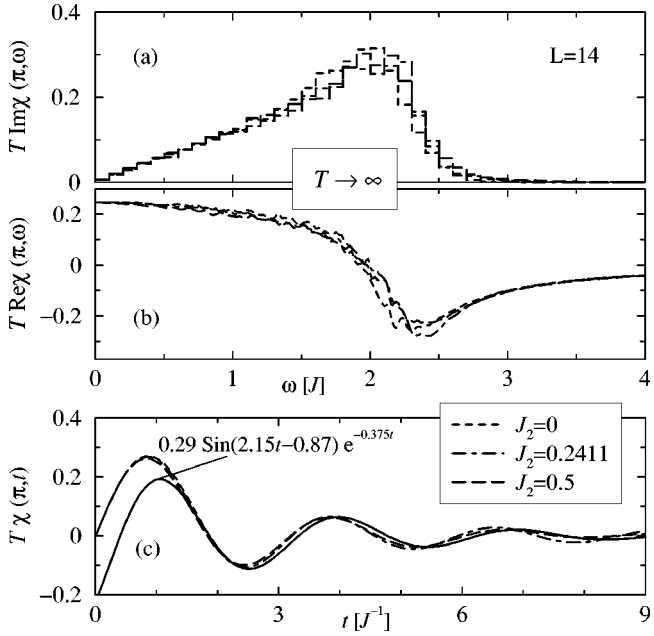

FIG. 17. Imaginary (a), real (b), and real-time (c) representation of the susceptibility for $T\to\infty$. Broken lines in (a) are binned, in Eq. (6) with $\epsilon=0.02$ was applied, and in (c) Eq. (8). The solid line in (c) is the sinusoidal fit for the example of $J_2=0$.

tion functions. The onset of this effect is already observed at $T=0.3$ as discussed in the previous sections. At $T=0.7$ the exponent of the upper continuum edge for $J_2=0$ is $\alpha=3.2(1)$ so that the singularity is basically completely damped out. Also, the rather large effective continuum edge $\Lambda=3.45(10)$ does not quite reproduce the correct oscillatory behavior as a function of time.

At about the same temperature the scaling dimension increases to $x\sim 1$. $T^*\approx 0.7$ thus marks the crossover temperature from strongly interacting, conformally invariant to noninteracting fermion and high-energy diffusive behavior. This is consistent with $\partial_T \mathrm{Re}\,\chi(\pi,\infty)$ and $\partial_T \mathrm{Re}\,\chi(\pi,3.8)$ being extremal at $T\approx T^*$ as seen in Figs. 3 and 5.

Figure 16(c) shows the real-time representation of the spin-correlation function of the unfrustrated Heisenberg chain at $T=1$. The amplitude of the modulations between $tJ\approx 2$ and the onset of finite-size effect for the 14-site chain at $tJ\sim 7$ cannot be fitted algebraically. The exponential fit from Eq. (28) shown by the full line in Fig. 16(c) matches excellently. The analogy to the XY model suggests that the long-time asymptotics is captured in this fit. The extracted value for $\Lambda=2.31(1)$ thus marks the effective, thermally smeared out upper band edge. For the appropriate interpretation of the parameter $\Gamma=0.941(5)$ refer to Sec. IV.

The discrepancy of the real-time fit function [full line in Fig. 16(c)] and the correct line shape for small times does not allow for a direct comparison of the results with its Fourier transforms. The difference between the fit and the exact result is roughly exponential. The fit with Eq. (28) implies that the real and imaginary part should contain contributions from the continuum boundary Lorentzians Eqs. (27) and (25). Indeed, the double Lorentzian fits [full lines in Figs. 16(a) and 16(b)] with an additive Lorentzian contribution centered at $\omega=0$ compare well with the binned data for the imaginary part and the real-part data from Eq. (6) with $\epsilon=0.03$ (broken lines). The fit parameters even though similar are not such that the fits are appropriately Kramers-Kronig and Fourier related. The fits must thus be regarded as sophisticated guides to the eye. Similar results are obtained for $J_2>0$. Similar line shapes are also found in systems with large spins.[40]

F. High-temperature limit

In Figs. 17(a), 17(b), and 17(c) we show the respective imaginary, real, and real-time representation of the susceptibility for different values of the frustration in the limit of infinite temperatures. The data of the imaginary part (a) are binned and the real part (b) is given by Eq. (6) with $\epsilon=0.02$ for $L=14$. The time representations (c) from Eq. (8) show finite-size effects for $t>6/J$.

For $\omega\to 0$ the slopes of the imaginary part are similar to the exact result for the XY model Eq. (29). A small frustration dependence becomes obvious when plotting the structure factor instead of the correlation function.[8,9]

The oscillations in time shown in Fig. 17(c) can be fitted very accurately for $1.5<tJ<6$ with an exponential decay via Eq. (28). The parameter sets $[\Lambda,\Gamma,\phi]$ are obtained as $[2.15(1),0.375(2),-0.87(1)]$ for $J_2=0$, $[2.31(1),0.323(2),-1.13(1)]$ for $J_2=0.2411$, and $[2.21(1),0.345(2),-0.82(1)]$ for $J_2=0.5$. The full line shows the resulting fit function for $J_2=0$.

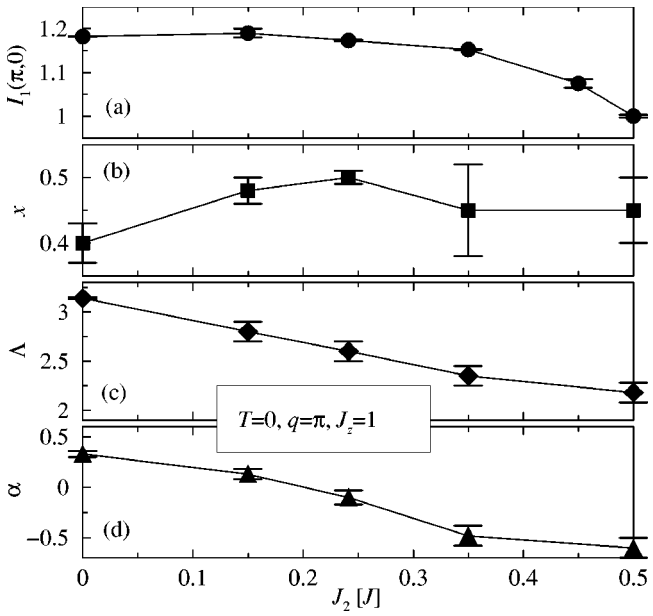

FIG. 18. Extracted values for (a) the sum rule $I_1(\pi,0)$, (b) the scaling dimension x, (c) the upper edge of the continuum, and (d) the exponent at the upper edge of the continuum as a function of J_2 at $T=0$.

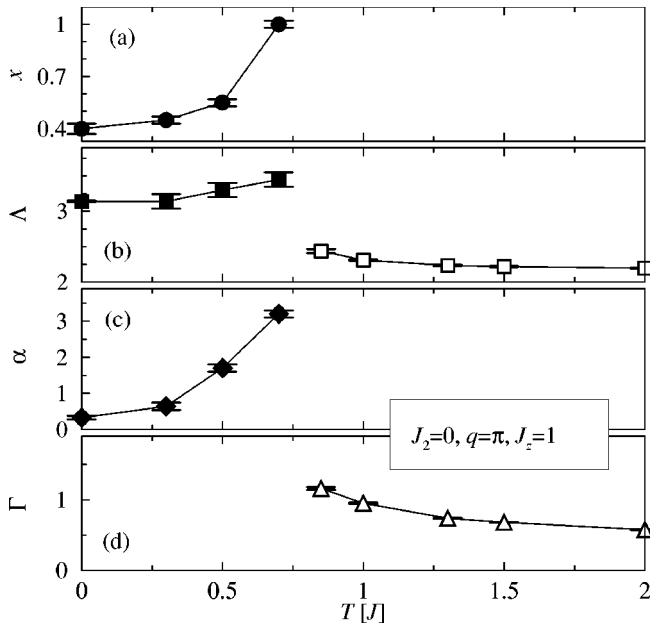

FIG. 19. Extracted values for (a) the scaling dimension x for $T<T^*$, (b) the upper-continuum cutoff frequency for $T<T^*$ (full symbols) and the effective upper continuum edge in the diffusive/weakly interacting-fermion regime (open symbols), (c) the cutoff exponent, and (d) the control parameter Γ determining the decay as a function of time in the diffusive/weakly interacting-fermion regime.

In the classical limit, where $\langle S_z^2\rangle_{T\to\infty}\to\infty$, paramagnetic behavior is expected for $T\gg J$. This leads to an expected functional dependence of the structure factor of $\lim_{T\to\infty}S_{\rm class}(q,\omega)\sim\lim_{\epsilon\to 0}\epsilon/(\omega^2+\epsilon^2)$. From Eq. (35) follows that $\lim_{T\to\infty}T\,\mathrm{Re}\,\chi(\pi,0)=\langle S_z^2\rangle_{T\to\infty}$ that is consistent with the expected functional dependence in the classical limit.

The XY model is one point of the line of critical fixed points towards that the interaction flows in a bosonized representation of the Heisenberg model.[31,32] The susceptibility of the XY model shows a square-root divergence at $\omega=2$ and $\mathrm{Im}\,\chi_{XY}(\pi,\omega>2)\equiv 0$. The shape of the spectrum at the upper band edge observed for Heisenberg chains is thus an interaction effect.[8] The shape of $\mathrm{Im}\,\chi(\pi,\omega\sim\Lambda)$ indeed resembles that of a Fermi distribution of weakly interacting electrons. We thus interpret the limit $T\to\infty$ as best described by weakly interacting spinless fermions.

IV. RESULTS

Figure 18 summarizes as a function of the frustration J_2 at $T=0$ the extracted values for (a) the sum rule $I_1(\pi,0)$, (b) the scaling dimension x, (c) the upper edge of the continuum Λ, and (d) the exponent at the upper edge of the continuum α.

(a) The values of I_1 for $J_2\leqslant 0.2411$ are within error bars almost identical that underlines the common features of Heisenberg chains with undercritical frustration.[14,15,31,32]

(b) The parameter x shows a stronger infrared divergence for unfrustrated Heisenberg chains than for those with critical frustration. Our results with $x<0.5$ are consistent with scaling dimension $x=0.5$ and additional logarithmic corrections. The values for overcritical frustration have to be regarded as effective ones as discussed in Sec. III C.

(c) The cutoff frequency of the upper limit of the spinon continuum is linear as a function of frustration for $J_2<0.35$.

(d) The exponent of the cusp at the upper boundary of the spinon continuum is always smaller than the value of $\alpha=0.5$ predicted for the two-spinon contribution for J_2. The value of α vanishes for $J_2\approx 0.2$ in agreement with the previous observation[5] that for that value the spectral properties of the frustrated Heisenberg chain are similar to the conformally invariant Haldane-Shastry[41,42] model.

The prefactor χ_0 from Eq. (13) is of order 1 and slightly frustration dependent. The values (J_2,χ_0) are: $(0,1.31(5))$, $(0.15,1.12(5))$, $(0.2411,1.01(5))$, and $(0.35,0.88(5))$. For $J_2=0.5$ one has $v^{1-2x}\chi_0=0.69(5)$. Values for $J_2=0.45$ are not computed because of the peculiar finite-size effects shown in Fig. 3.

Figure 19 summarizes the temperature dependence of the fit parameters for the experimentally most relevant unfrustrated chain with $J_2=0$.

(a) The scaling variable approaches the value of the XY model limit at the crossover temperature to the diffusive regime $T^*\approx 0.7$. The direct determination of $x(T>T^*)$ is not possible but since for $T\to\infty$ the weakly interacting fermion case is recovered it is expected to lock in at $x(T>T^*)=1$.

(b) The upper continuum edge $\Lambda(T<T^*)$ marks a sharp cutoff (full symbols) while in the diffusive regime (open symbols) it is the effective, thermally smeared out upper continuum boundary. In the weakly interacting fermion limit it saturates at $\Lambda(T\to\infty)=2.15(1)$.

(c) The exponent of the upper continuum edge α in-

creases with increasing temperature reflecting the thermal smearing out of the singularity. Its value at $T=T^*$ is so large that the cutoff is barely singular and thus not very well defined. In the diffusive regime ($T>T^*$) this quantity is undefined.

(d) Γ is an effective parameter that controls the continuous transition of the system from the diffusive behavior at T^* to the weakly interacting fermion limit at $T\rightarrow\infty$. For $J_2=0$ it saturates at $\Gamma(T\rightarrow\infty)=0.375(2)$

V. CONCLUSIONS

We have compared numerical results from the exact diagonalization of finite systems with results from conformal-field theory together with implications from the density of states, the exactly solvable XY model, and Bethe ansatz solutions for integrable systems. We use the different finite-size accuracy of the imaginary, real, and time representations of the spin-correlation functions to extract reliable information on the thermodynamic limit.

At low temperatures the dynamical correlation functions of frustrated Heisenberg chains are well described by a multiplicative superposition of the contribution from low-lying elementary excitations described by conformal-field theory and a density of states and matrix-element-induced singularity near the upper edge of the two-spinon continuum. At the frustration value of $J_2\approx 0.2$ the system is closest to the conformally invariant Haldane-Shastry model.

At $T^*\approx 0.7$ we observe the crossover from the low temperature, conformally invariant regime to a diffusive regime. All correlations in time then decay exponentially. The diffusive regime connects continuously to the weakly interacting fermion regime for $T\rightarrow\infty$.

We give the frustration dependence of the control parameters for the lineshapes of the spin-correlation functions at $T=0$ and their temperature dependence for the experimentally most relevant case of $J_2=0$. The temperature dependence of the first moment sum rule of the spin-correlation function is accurately determined.

ACKNOWLEDGMENTS

We are grateful to H. Yokoyama for giving us access to the data published in Ref. 5. We thank I.A. Zaliznyak, J. Stolze, F.H.L. Essler, V.J. Emery, and M. Weinert for stimulating and instructive discussions. The work performed at BNL was supported by DOE Contract No. DE-AC02-98CH10886.

[1] M. Karbach and G. Müller, Comput. Phys. **11**, 36 (1997).
[2] M. Karbach, K. Hu, and G. Müller, Comput. Phys. **12**, 565 (1998).
[3] D. Augier, D. Poilblanc, S. Haas, A. Delia, and E. Dagotto, Phys. Rev. B **56**, 1997 (1997).
[4] S. Haas and E. Dagotto, Phys. Rev. B **52**, 14 396 (1995).
[5] H. Yokoyama and Y. Saiga, J. Phys. Soc. Jpn. **66**, 3617 (1997).
[6] D. Poilblanc, J. Riera, C.A. Hayward, C. Berthier, and M. Horvatic, Phys. Rev. B **55**, 11 941 (1997).
[7] D. Augier and D. Poilblanc, Eur. Phys. J. B **1**, 19 (1998).
[8] K. Fabricius, U. Löw, and J. Stolze, Phys. Rev. B **55**, 5833 (1997).
[9] K. Fabricius and U. Löw, Phys. Rev. B **57**, 13 371 (1998).
[10] O.A. Starykh, A.W. Sandvik, and R.R.P. Singh, Phys. Rev. B **55**, 14 953 (1997).
[11] G. Müller, H. Thomas, H. Beck, and J.C. Bonner, Phys. Rev. B **24**, 1429 (1981).
[12] H.J. Schulz, Phys. Rev. B **34**, 6372 (1986). The original result is found in A. Luther and I. Peschel, Phys. Rev. B **12**, 3908 (1975).
[13] A. M. Tsvelik, *Quantum Field Theory in Condensed Matter Physics* (Cambridge University Press, Cambridge, 1995).
[14] V.J. Emery and C. Noguera, Phys. Rev. Lett. **60**, 631 (1988).
[15] R. Chitra, S. Pati, H.R. Krishnamurthy, D. Sen, and S. Ramasesha, Phys. Rev. B **52**, 6581 (1995).
[16] Y. Yu, G. Müller, and V. Viswanath, Phys. Rev. B **54**, 9242 (1996).
[17] M. Karbach, G. Müller, A.H. Bougourzi, A. Fledderjohann, and K.-H. Mütter, Phys. Rev. B **55**, 12 510 (1997).
[18] O.A. Starykh, R.R.P. Singh, and A.W. Sandvik, Phys. Rev. Lett. **78**, 539 (1997).
[19] M. Karbach, K. Hu, and G. Müller, cond-mat/0008018 (unpublished).
[20] M. Karbach and G. Müller, Phys. Rev. B **62**, 14 871 (2000).
[21] R. Werner, Phys. Rev. B **63**, 174416 (2001).
[22] T. Ami, M.K. Crawford, R.L. Harlow, Z.R. Wang, D.C. Johnston, Q. Huang, and R.W. Erwin, Phys. Rev. B **51**, 5994 (1995).
[23] N. Motoyama, H. Eisaki, and S. Uchida, Phys. Rev. Lett. **76**, 3212 (1996).
[24] R. Coldea, D.A. Tennant, R.A. Cowley, D.F. McMorrow, B. Dorner, and Z. Tylczynski, J. Phys.: Condens. Matter **8**, 7473 (1996).
[25] D.A. Tennant, R.A. Cowley, S.E. Nagler, and A.M. Tsvelik, Phys. Rev. B **52**, 13 368 (1995).
[26] R. Werner, Ph.D. thesis, Dortmund, 1999.
[27] A. Fledderjohann and C. Gros, Europhys. Lett. **37**, 189 (1997).
[28] S. Eggert, Phys. Rev. B **54**, R9612 (1996).
[29] K. Okamoto and K. Nomura, Phys. Lett. A **169**, 433 (1992).
[30] E. F. Fradkin, *Field Theories of Condensed Matter Systems* (Addison-Wesley, New York, 1991).
[31] V. J. Emery, in *Highly Conducting One-Dimensional Solids*, edited by J. T. Devreese, R. P. Evrard, and V. E. van Doren (Plenum, New York, 1979), p. 247.
[32] K. Nomura and K. Okamoto, J. Phys. A **27**, 5773 (1994).
[33] The requirement of the spectrum to be bounded can be relaxed to $\lim_{\omega\rightarrow\infty}\mathrm{Im}\,\chi(q,\omega)\sim\omega^{-s}$ with $s>2$. For $s=2$ there will be logarithmic corrections $\lim_{\omega\rightarrow\infty}\mathrm{Re}\,\chi(q,\omega)\sim\omega^{-2}\ln[\omega^{-1}]$.
[34] C.K. Majumdar and D.K. Ghosh, J. Math. Phys. **10**, 1388 (1969).
[35] Interestingly, the spectral lines from the singlet excitations relevant for the dimer-dimer correlation functions (Ref. 21) and the triplet excitations are degenerate (Ref. 29) for $J_2=J_c$.

[36] For practical purposes this discrepancy can be overcome for smallfrequencies by rescaling the frequency dependence as has been done in the case of dimer-dimer correlation functions (see Ref. 21).
[37] J. des Cloizeaux and J.J. Pearson, Phys. Rev. **128**, 2131 (1962).
[38] B.S. Shastry and B. Sutherland, Phys. Rev. Lett. **47**, 964 (1981).
[39] G. Uhrig, *Niedrigdimensionale Spinsysteme und Spin-Phonon-Kopplung* (Habilitation, Cologne, 1999).
[40] J. Villain, J. Phys. (France) **35**, 27 (1974).
[41] F.D.M. Haldane, Phys. Rev. Lett. **60**, 635 (1988).
[42] B.S. Shastry, J. Stat. Phys. **50**, 57 (1988).